Thin heterogeneous SOI waveguides for thermo-optical tuning and filtering

Andrei V. Tsarev [1], Francesco De Leonardis [2] and Vittorio M. N. Passaro [3*]

[1] *Institute of Semiconductor Physics, Siberian Branch Russian Academy of Sciences*
Prospect Lavrenteva, 13, Novosibirsk, 630090, Russia
tsarev@.isp.nsc.ru
[2] *Photonics Research Group, Dipartimento di Ingegneria dell'Ambiente e per lo Sviluppo Sostenibile, Politecnico di Bari, viale del Turismo n. 8, 74100 Taranto, Italy*
f.deleonardis@poliba.it
[3] *Photonics Research Group, Dipartimento di Elettrotecnica ed Elettronica, Politecnico di Bari, via Edoardo Orabona n. 4, 70125 Bari, Italy, URL: http://dee.poliba.it/photonicsgroup*
** Corresponding author: passaro@deemail.poliba.it*

Abstract: This work presents an analysis and simulation of novel heterogeneous silicon-on-insulator (SOI) waveguide structures for reconfigurable optical add/drop multiplexers (ROADMs) with thermo-optic tuning and multi-reflector beam expanders. New structure design includes p^+ side-doping of SOI ridge waveguide with 220 nm×16 μm silicon core. It provides quasi mono-mode behavior due to strongly mode-dependent optical losses by free charge absorption. These silicon heterogeneous waveguides are used to investigate ROADMs including nano-structured 2D-gratings for fiber coupling and polarization diversity, nano-grooves or p^+ doping reflector strips for multi-reflector beam expanders and local heaters for wideband thermo-optic tuning.

OCIS codes: (060.1810) Couplers, switches, and multiplexers; (130.0130) Integrated optics; (130.3120) Integrated optics devices; (130.5990) Semiconductors; (160.6840) Thermo-optical materials.

References and links

1. W. Bogaerts, D. Taillaert, P. Dumon, D. Van Thourhout, and R. Baets, "A polarization-diversity wavelength duplexer circuit in silicon-on-insulator photonic wires," Opt. Express **15**, 1567-1578 (2007).
2. W. Bogaerts, P. Dumon, D. Van Thourhout, D. Taillaert, P. Jaenen, J. Wouters, S. Beckx, and R. Baets, "Compact wavelength-selective functions in silicon-on-insulator photonic wires," IEEE J. Sel. Top. Quantum Electron. **12**, 1394-1401 (2006).
3. P. Dumon, W. Bogaerts, D. Van Thourhout, D. Taillaert, R. Baets, J. Wouters, S. Beckx, and P. Jaenen, "Compact wavelength router based on a silicon-on-insulator arrayed waveguide grating pigtailed to a fiber array," Opt. Express **14**, 664–669 (2006).
4. T. Fukazawa, F. Ohno, and T. Baba, "Very compact arrayed-waveguide grating demultiplexer using Si photonic wire waveguides," Jpn. J. Appl. Phys. **43**, L673–L675 (2004).
5. J. Floriot, F. Lemarchand, and M. Lequime, "Tunable double-cavity solid-spaced bandpass filter," Opt. Express **12**, 6289-6298 (2004).
6. Y. Zhu, P. Shum, C. Lu, P. Swart, B. Lacquet, and S. Spammer, "Promising compact wavelength-tunable optical add-drop multiplexer in dense wavelength-division multiplexing systems," Opt. Lett. **29**, 682-684 (2004).
7. C. Doerr, L. Stulz, D. Levy, R. Pafchek, M. Cappuzzo, L. Gomez, A. Wong-Foy, E. Chen, E. Laskowski, G. Bogert, and G. Richards, "Wavelength add–drop node using silica waveguide integration," J. Lightwave Technol. **22**, 2755-2762 (2004).
8. P. Tang, O. Eknoyan, and H. Taylor, "Rapidly Tunable Optical Add-Drop Multiplexer (OADM) using a static-strain-induced grating in $LiNbO_3$," J. Lightwave Technol. **21**, 236-245 (2003).
9. L. Eldada, "Polymer integrated optics: promise versus practicality," Proc. SPIE **4642**, 11-22 (2002).
10. S. Toyoda, N. Ooba, T. Kitoh, T. Kurihara and T. Maruno, "Wide tuning range and low operating power AWG-based thermo-optic wavelength tunable filter using polymer waveguides," Electron. Lett. **37**, 1130-1132 (2001).
11. V. M. N. Passaro, F. Magno, and A. Tsarev, "Investigation of thermo-optic effect and multireflector tunable filter/multiplexer in SOI waveguides," Opt. Express **13**, 3429-3437 (2005).

#90953 - $15.00 USD Received 17 Dec 2007; revised 25 Jan 2008; accepted 28 Jan 2008; published 21 Feb 2008

12. W. Bogaerts, R. Baets, P. Dumon, V. Wiaux, S. Beckx, D. Taillaert, B. Luyssaert, J. Van Campenhout, P. Bienstman, and D. Van Thourhout "Nanophotonic waveguides in silicon-on-insulator fabricated CMOS technology," J. Lightwave Technol. **23**, 401-412 (2005).
13. A. V. Tsarev, "New type of heterogeneous nanophotonic silicon-on-insulator optical waveguides," Quantum Electron. (Rus) **37**, 775-776 (2007).
14. A. V. Tsarev, V. M. N. Passaro, and F. Magno, "Widely tunable reconfigurable optical add/drop multiplexers in silicon-on-insulator technology: a new approach," in *Silicon Photonics*, V. M. N. Passaro, ed., (Research Signpost publisher, Kerala, India, 2006) 47-77. ISBN: 81-308-0077-2
15. A. V. Tsarev "Peculiarity of multi-reflector filtering technology," Proc. 13th European Conf. on Integrated Optics and Technical Exhibition, Copenhagen, Denmark, ThG23 (2007).
16. A. V. Tsarev, "Tunable optical filters," United States Patent No 6,999,639, February 14, 2006.
17. A. V. Tsarev, "Beam-expanding device," United States Patent No 6,836,601, December 28, 2004.
18. Comsol Multiphysics by COMSOL ©, ver. 3.2, single license (2005).
19. BeamProp 8.0 and FullWave 6.0 by RSoft Design Group Inc., single license (2007).
20. D. Taillaert, H. Chong, P. Borel, L. Frandsen, R. De La Rue and R. Baets, "A compact two-dimensional grating coupler used as a polarization splitter," IEEE Photon. Technol. Lett. **15**, 1249–1251 (2003).
21. R. A. Soref and B. R. Bennett, "Electrooptical effects in silicon," IEEE J. Quantum Electron. **QE-23**, 123-129 (1987).
22. G. Cocorullo, M. Iodice, and I. Rendina, "All-silicon Fabry–Perot modulator based on the termo-optic effect," Opt. Lett. **19**, 420–422 (1994).

Introduction

Reconfigurable optical add/drop multiplexers (ROADMs) are among the most demanded devices that can increase flexibility and capacity of wavelength-division-multiplexing (WDM) fiber optical networks. Although a great progress has been achieved in recent years [1-12], none of actual technologies could be regarded as ideal to substitute each other in the near future. The research effort is mainly focused on silicon-on-insulator (SOI) structures, due the great advantages of silicon for photonic devices. Successful CMOS compatible technology for optical add/drop multiplexers in SOI [1-4, 12] makes possible the development of reconfigurable devices. The significant problem derives from the physical constraints to achieve controllable changes of silicon refractive index. This limits the possible tuning range to a small fraction of WDM transmitted band. Thus, ROADMs could not be realized in SOI for perspective flexible fiber optical networks using multi-hundreds wavelength channels.

In order to reduce the cost per channel needed for the commercialization of WDM systems, integrated tunable optical filters and ROADMs based on patented multi-reflector (MR) filtering technology have been already proposed [13-16]. Their advantages consist of the unique opportunity of optical wavelength wide tuning within total C- or L-bands of WDM networks [14]. This technology combines physical phenomena of wave-guiding, reflection and constructive interference in a novel way, by spatially expanding the optical beam through a patented MR-beam expander (BE) [17], then tuning and filtering the desired wavelength by a set of tunable channel waveguides (see Fig. 1) and by constructive interference of multiple sub-beams, combined at the output channel waveguide (Drop or Through) by another beam expander [14].

Multi-reflector technology provides the possibility of developing tunable devices, thermo-optic filters (TOF) and ROADM, on different materials (silicon, polymer, lithium niobate) [11, 14, 15], allowing partial reflector manufacturing, optical phase tunability and low optical losses in single-mode waveguides. In principle, MR-filtering devices could be fabricated by modern nanophotonics CMOS-compatible technology, as for silicon-on-insulator structures [1-4, 12]. However, nowadays MR-devices have not yet been studied experimentally and its theoretical study is still under investigation, containing a lot of unresolved aspects.

This paper describes the new heterogeneous optical waveguide [13], i.e. a SOI nanostrip having 220 nm×16 μm silicon core and both doped sides, and its application for novel types of ROADM structures. Structure design is accomplished by a number of numerical simulations using finite element method (FEM) [18], beam propagation method (BPM) and finite difference time domain (FDTD) method [19]. To have faster simulations, 3D structure has been replaced by its two-dimensional (2D) analogy using the effective index method (EIM), that decomposes 3D strip waveguide into two 2D slab waveguides.

#90953 - $15.00 USD Received 17 Dec 2007; revised 25 Jan 2008; accepted 28 Jan 2008; published 21 Feb 2008

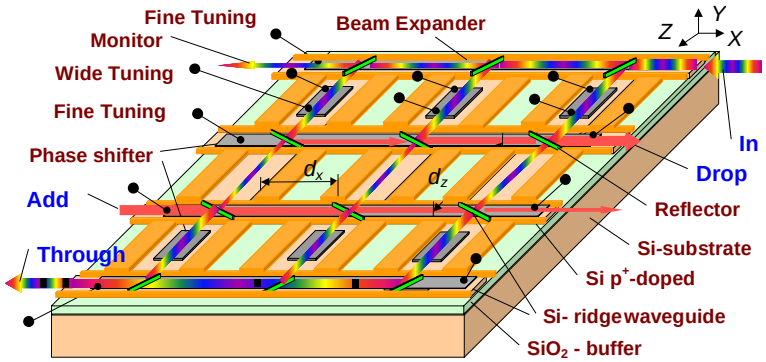

Fig. 1. General view of thermo-optic MR-ROADM in SOI technology.

1. Heterogeneous waveguide in thin SOI

Recently, nano-scale 2D grating etched in a thin SOI waveguide [20] has been used as a fiber-to-ridge waveguide coupler. This grating is compatible with new heterogeneous optical waveguides [13] and both of them are perspective for multi-reflector technology, as they provides the additional possibility of polarization diversity without polarization rotators [1]. This 2D grating element is very compact and couples orthogonal modes from a single-mode optical fiber into two quasi-TE modes of two crossed ridge waveguides, that could be connected to the input/output of the photonic integrated circuit. However, the thin (220 nm) ridge waveguide can be very large (compatible to fiber core), i.e. 10 μm, so experiencing a strongly multi-mode behavior due to its high index contrast, at the expenses of device performance.

Here we briefly describe optical properties of recently proposed [13] heterogeneous optical waveguides (see Fig. 2) and, then, different architectures that are very suitable for SOI devices. EIM approximation (i.e. 2D analogy) of this heterogeneous 3D waveguide structure corresponds to a core refractive index of 2.852.

A simple relation between changes of real part of refractive index (Δn) and absorption ($\Delta\alpha$) at the wavelength of interest (λ_0 = 1.55 μm), due to presence of free electron (N_e) and hole concentration (N_h), can be derived in silicon as [21]:

$$\Delta\alpha_e = 0.12\times|\Delta n_e| \qquad (1)$$

$$\Delta\alpha_h = 0.16\times|\Delta n_h|^{5/4}$$

Thus, the total change of complex refractive index due to the charge effect is:

$$\Delta n_c = \Delta n + in' \qquad (2)$$

where $n' = \Delta\alpha\lambda_0/(4\pi)$, $\Delta n = \Delta n_h + \Delta n_e$, $\Delta\alpha = \Delta\alpha_h + \Delta\alpha_e$.

From Eq. (1) one can see that, if $\Delta n < 0.3$, then the hole doping is more preferable as it provides smaller optical losses for the same index change, with quality factor $|\Delta n_h|^{1/4}$, which describes ratio of the additional optical losses for the same index increment $\Delta n_h = \Delta n_e$, that could be obtained by appropriate electron and holes free charge concentrations. Thus, we propose to use p^+-doping for all structures discussed below, with a doping level of the order of 10^{18} cm^{-3}. Quasi single-mode behavior of thin ridge waveguides could be achieved by manufacturing heavily doped p^+-regions on both sides of the silicon ridge (see Fig. 2) [15]. Through an optimum choice of both waveguide sizes and doping level, it is possible to obtain the fundamental mode as mainly confined in the lossless central region (width W). On the

#90953 - $15.00 USD Received 17 Dec 2007; revised 25 Jan 2008; accepted 28 Jan 2008; published 21 Feb 2008

contrary, the other higher order modes will spread out to the total heterogeneous waveguide ($W+2 \cdot W_g$ wide), including the high loss regions due to free charge absorption (see Fig. 3).

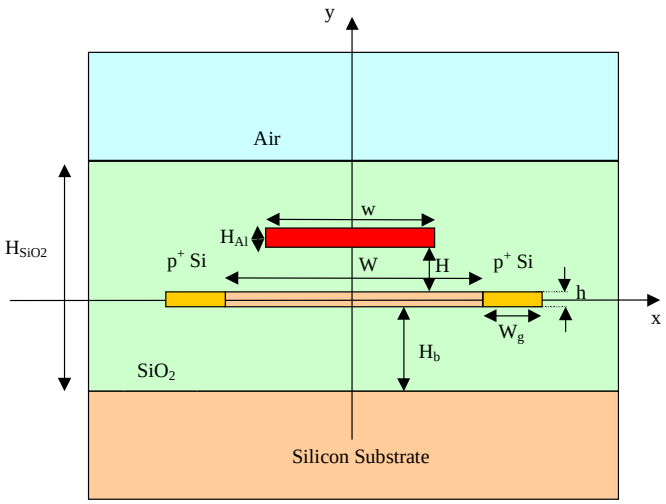

Fig. 2. Heterogeneous SOI waveguide. Parameters are h=220 nm, H_b = 1 μm ,W = 6-10 μm, W_g = 4-8 μm, H_{SiO2} = 2 μm, H_{Al} = 0.2 μm, N_{si} = 3.478, N_{si02} = 1.447.

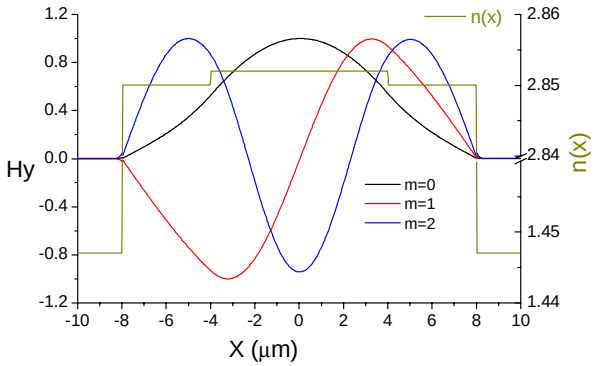

Fig. 3. Re[n(x)] and mode field distribution of heterogeneous SOI waveguide (W = 8 μm, W_g = 4 μm). Effective indices are N_m=2.851325+0.0000065i (m = 0), N_m = 2.849507+0.0000244i (m = 1), N_m= 2.847083+0.0000417i (m = 2). Simulations made by 2D BPM mode solver [19].

Complex effective indices N_m of guided modes in heterogeneous SOI waveguides have been found by 2D BPM mode solver [19]. Imaginary part of N_m gives the optical loss. In order to verify the validity of BPM approximation, we have compared these results with FDTD simulations of the same waveguide. Guided modes found by 2D BPM mode solver, as presented in Fig. 3, have been launched into 2D waveguide and overlap integrals of FDTD field with these modes have been evaluated at different propagation lengths (100 μm, 200 μm and 300 μm). This procedure gives the waveguide optical losses. The BPM simulation gives almost the same values for optical losses (see Table 1), that well demonstrates the validity of BPM approximation for the proposed heterogeneous SOI waveguides. A more detailed investigation of optical losses for different waveguide structures is presented in Fig. 4. It shows that fundamental mode of the homogeneous ridge waveguide has negligible losses with respect to higher order modes.

#90953 - $15.00 USD Received 17 Dec 2007; revised 25 Jan 2008; accepted 28 Jan 2008; published 21 Feb 2008

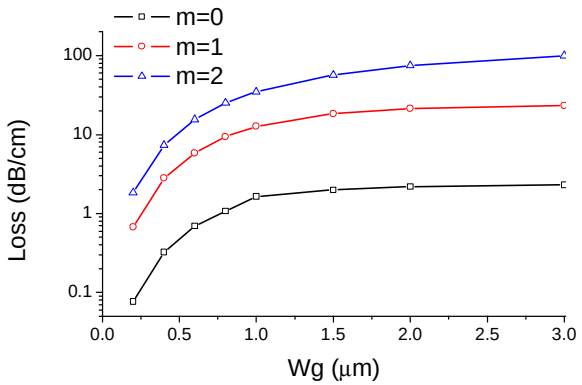

Fig. 4. Optical losses for different modes of ridge waveguide as a function of $p+$ doped regions width W_g. Simulations made by 2D BPM mode solver [19].

Table 1. Comparison of 2D BPM and FDTD simulations for the structure in Fig.3.

m	Re (N_m)	Im (N_m)	$Loss_{BPM}$	$Loss_{FDTD}$
0	2.851328	6.48E-06	2.3	2.4
1	2.849522	2.47E-05	8.7	8.8
2	2.847135	4.23E-05	14.9	15.0

2. Partial reflectors in thin SOI

Heavily doped p^+-regions could be also used for fabrication of slanted reflectors in widely tuned MR-ROADM [14]. Dependence of reflected and transmitted power on the doped region width W_g for an incident angle 75° is shown in Fig. 5. Although the additional absorption losses are noticeable, it provides possibility to manufacture devices with suitable performance.

An alternative method to fabricate partial reflectors for MR-ROADM should be based on deep groove technology combined with back filling of the groove by using a material with appropriate refractive index, in order to provide small reflection coefficient. For a quasi-TE mode incident on the reflector at its Brewster angle, reflection coefficient could be sufficiently small even for high index contrast silicon-air interface, that should make possible to eliminate complex groove back filling. Besides, results presented in Fig. 6 show that the reflection coefficient for nano-width grooves could precisely be controlled by changing both thickness and angle of the groove. Of course, the reflected field is distorted at Brewster angle and energy of fundamental mode is less than the total reflected power, due to the presence of higher order modes. As it was noted before, these modes decay due to the presence of both heavy doped sides of the ridge waveguide.

3. Thermo-optic phase shifters in thin SOI

We have carried out static and dynamic thermo-optical analysis of thin heterogeneous waveguide by FEM [18], by a fully integrated 2D thermo-optic simulation.

In general, to solve a particular heat conduction problem and find the temperature distribution, it is necessary to specify the medium geometry and thermo-physical properties, the distribution of possible sources and the initial and boundary conditions. These conditions are essentially of two types: Dirichlet, where a temperature is imposed on the medium surface, as $T = T_0$, or Neumann, where the heat flux q on a boundary is fixed as $- \boldsymbol{n} \cdot \boldsymbol{q} = q_0$, where $\boldsymbol{n}$ stands for the surface normal. The heat flux is defined by the Fourier law as:

$$\boldsymbol{q} = - k \nabla T \tag{3}$$

#90953 - $15.00 USD Received 17 Dec 2007; revised 25 Jan 2008; accepted 28 Jan 2008; published 21 Feb 2008

where the negative sign is justified by the opposite directions of heat flux and temperature gradient. Absence of any generation terms and scalar conductivity for both static and dynamic analysis have been assumed.

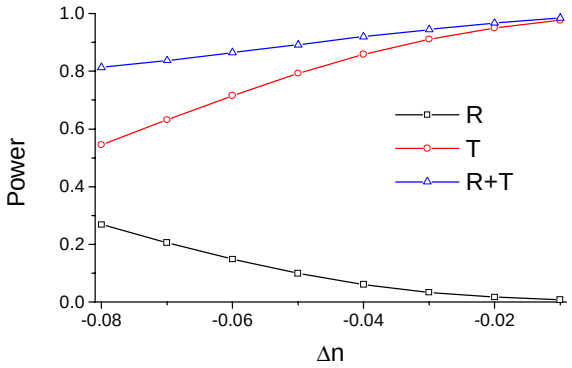

Fig. 5. Dependence of power reflection and transmitting coefficients as a function of $\Delta n = \Delta n_h$. (2D FDTD simulation).

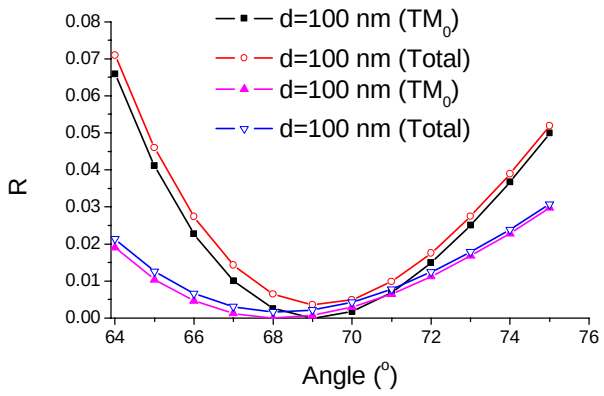

Fig. 6. Amplitude of power reflection coefficient for fundamental TM_0 mode as a function of incident angle on the deep groove. Solid dots describes reflection only for the fundamental TM_0 mode. Open dots describe the reflection coefficient for all modes (2D FDTD simulation, waveguide width 10 μm).

Table 2 summarizes the thermo-physical values used in the simulations for the materials involved in the waveguide. In this work, constant values for conductivity, density and heat capacity of the air are used.

Table 2. Thermo-physical constants used in the simulations [22].

Material	k [W/m·K]	P [kg/m^3]	C [J/kg·K]	∂n/∂T
Silicon	163	2330	703	$1.86\ 10^{-4}$
Silica	1.38	2203	703	$1.477\ 10^{-5}$
Aluminum	160	2700	900	-
Air (@ 30°C)	0.026	1.166	1005	-

The effective thermo-optic coefficient depends on the waveguide materials (refractive index, density, heat capacity, thermal conductivity), geometry, temperature gradient in each layer, heater material and width. If a guided-wave optical device employs the thermo-optic effect for switching, filtering or tuning operations, its characteristics depend on this effective

#90953 - $15.00 USD Received 17 Dec 2007; revised 25 Jan 2008; accepted 28 Jan 2008; published 21 Feb 2008

thermo-optic coefficient, that can be seen as a property of the whole waveguide structure. For example, in a Mach-Zehnder thermo-optic switch, the optimum heater length L_{eff} that corresponds to the phase shift π, is written as:

$$L_{eff} = \lambda \Big/ \left(2 \partial n \big/ \partial T \, \Delta T \right) \ . \tag{4}$$

By means of the dynamic analysis, we have evaluated the time dependence of the temperature and the effective index, so estimating the thermo-optic response time and switching power of the analyzed structures as:

$$P_{\pi} = q_o w L_{eff} \tag{5}$$

where w is the heater width and q_0 is the heat flux that is used in Neumann boundary condition. Results of the heat simulations are presented in Fig. 7-10.

Static simulation of the structure with constant heater temperature (Dirichlet boundary condition) is shown in Fig. 7 for H = 0.1 μm. One can see that the heat spreads not only along the waveguide but also into the silica surrounding, due to very thin silicon layer. Thus, the optimum heater dimension has to be optimized to the area of fundamental guided mode (~ W).

Important informations about thermo-optic phase shifter can be derived from dynamic simulations using FEM. We have analyzed heat spreading from the short (10 μs) rectangular impulse of inward heat flux [18], coming from the heater boundary with the SOI rib waveguide. Fig. 8 shows the time-dependent temperature variation in the center of the silicon core for different waveguide structures. The temperature impulse shape can be described by exponential functions with two different time decay parameters, namely τ_1 and τ_2:

$$\begin{aligned} T(t) &= T_0 && \text{for } t < t_1 \\ T(t) &= T_0 + \Delta T \{1 - \exp[-(t-t_1)/\tau_1]\} && \text{for } t_1 < t < t_2 \\ T(t) &= T_0 + \Delta T \exp[-(t-t_2)/\tau_2] && \text{for } t > t_2 \end{aligned} \tag{6}$$

where t_1 and t_2 are the time instants at the beginning and end of inward heat flux rectangular impulse, respectively. Moreover, ΔT is the maximum temperature increase in the waveguide core center and T_0 is the initial temperature, equal to the surrounded temperature (in this case 300 K°). The dynamic parameters of the waveguide heating and cooling are presented in Table 3. Heating process appears to be a little faster than cooling. The temperature increase ΔT and the time decay constants τ_1 and τ_2 do not depend on the distance (H) of the heater from the waveguide surface. However, the temperature in the waveguide core strongly depends on both heater width (w) and silica buffer height (H_b), thus significantly controlling the rate of heat flux from the heater to the silicon substrate. The spatial distribution of the temperature along the two orthogonal directions through the structure core center (as in Fig. 2) are presented in Fig. 9 and 10, respectively.

#90953 - $15.00 USD Received 17 Dec 2007; revised 25 Jan 2008; accepted 28 Jan 2008; published 21 Feb 2008

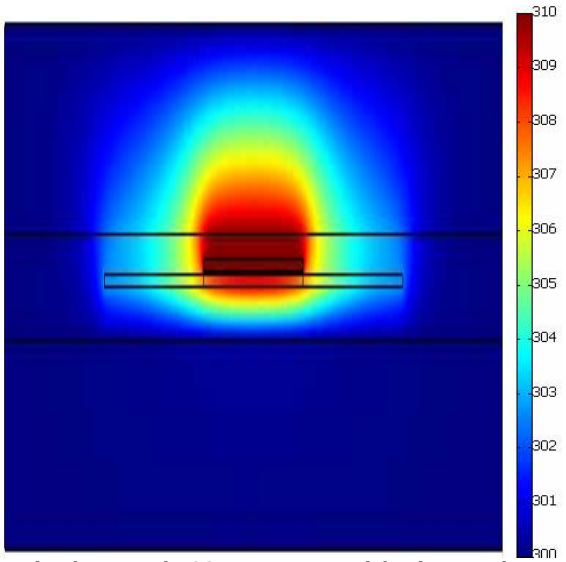

Fig. 7. Temperature distribution in the SOI structure around the aluminum heater (placed as in Fig. 2 with H = 0.1 μm). Heater temperature 310 K, surrounding temperature 300 K (w = 8 μm, W = 8 μm, W_g = 8 μm).

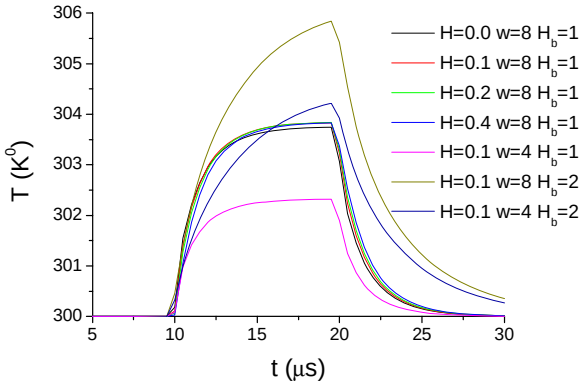

Fig. 8. Temperature response versus time in the center of SOI waveguide for various structure parameters. Inward heat flux is a step function impulse of 10 μs with an amplitude 10^{+7} W/m^2.

Table 3. Thermo-physical simulation of SOI structure.

H (μm)	H_b (μm)	w (μm)	W (μm)	W_g (μm)	T(core) K	Δn(core)	L_{eff} (μm)	P_π (mW)	τ_1 (μs)	τ_2 (μs)
0	1	8	8	8	303.74	0.0007	1114	89	1.27	1.62
0.1	1	8	8	8	303.83	0.00071	1088	87	1.34	1.56
0.2	1	8	8	8	303.84	0.00071	1086	87	1.41	1.61
0.4	1	8	8	8	303.82	0.00071	1090	87	1.54	1.70
0.1	1	4	8	8	302.32	0.00043	1798	72	1.18	1.42
0.1	2	8	8	8	305.84	0.00109	713	57	3.00	3.40
0.1	2	4	4	4	304.49	0.00084	927	37	3.32	3.59

A significant different behavior can be derived for the cases of heating and cooling, corresponding to the presence or absence of the input heat flux. The spatial distribution has

#90953 - $15.00 USD Received 17 Dec 2007; revised 25 Jan 2008; accepted 28 Jan 2008; published 21 Feb 2008

been used for simulation of the effective refractive index, determining the effective thermo-optic coefficient and switching power P_π in various cases, as in Table 3.

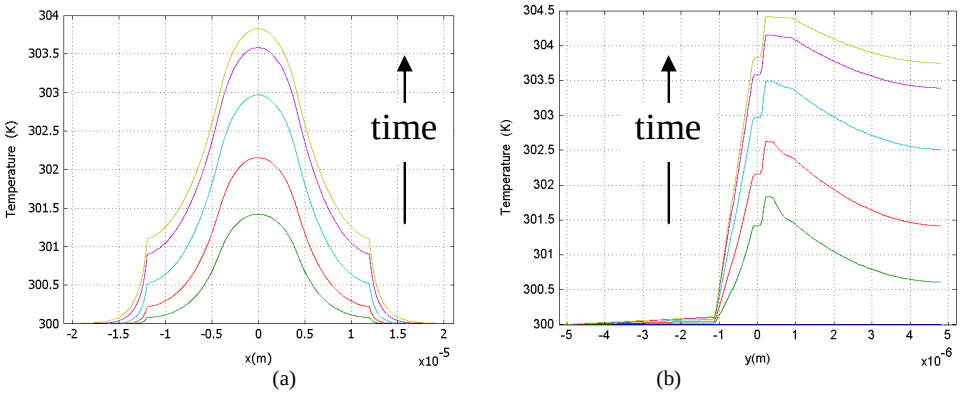

Fig. 9. Temperature distribution at different time instants (-2, 0.5, 1, 2, 4, 8 μs) in the SOI structure around the aluminum heater: a) as a function of x horizontal direction at y = 0; b) as a function of y vertical direction at x = 0. Time measured from the start of impulse with duration 10 μs (heating process). Inward heat flux 10^{+7} W/m^2, w = 8 μm, W = 8 μm, W_g = 4 μm.

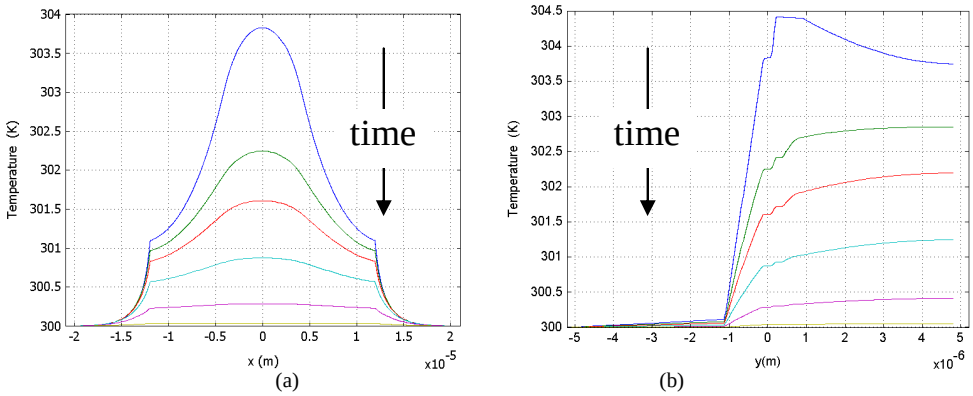

Fig. 10. Temperature distribution at different time instants (-2, 0.5, 1, 2, 4, 8 μs) in the SOI structure around the aluminum heater: a) as a function of x horizontal direction at y = 0; b) as a function of y vertical direction at x = 0. Time measured from the end of impulse with duration 10 μs (cooling process). Inward heat flux 10^{+7} W/m^2, w = 8 μm, W = 8 μm, W_g = 4 μm.

4. Multi-reflection technology in thin SOI

Optical elements shortly discussed above could constitute multi-reflector tunable multiplexers as presented in Fig. 1. Typical MR-ROADMs [15] contain four multi-reflector beam expanders [17], constituted by heterogeneous strip optical waveguide array crossed by periodically spaced partial reflector strips. Namely, between each couple of beam expanders a set of strip waveguides is included with crossing orientation with respect to the beam expanders, each one corresponding to a partial reflector and guiding the relevant partially reflected optical sub-beam [14]. Between crossing waveguides and beam expanders, the separating gap W_g of $p+$ doped region is provided.

The operation of thermo-optic MR-ROADM was already described [14]. Our counterpart Fig. 1 clearly shows the paths of optical beams in MR-ROADM approach. An optical beam containing multiple wavelength components in a wide spectral range comes from the input fiber to the first (In) beam expander. This optical beam is divided into two parts at each slanted partial reflector. The main optical beam (that carrying the largest amount of energy)

#90953 - $15.00 USD Received 17 Dec 2007; revised 25 Jan 2008; accepted 28 Jan 2008; published 21 Feb 2008

passes the reflector to go further to the next reflector, and the reflected optical beam (carrying the smallest amount of energy) turns its propagation direction and is coupled to the crossing optical waveguide. This beam expander transforms narrow optical beams into wide ones containing a large number of sub-beams, depending their amplitudes and phases on the optical properties of reflectors and effective index of relevant optical waveguides.

All these sub-beams arrive to the second beam expander (Drop), whose reflector strips are reversely slanted with respect to the In beam expander reflectors. Every sub-beam is split again into two parts at each partial reflector. One optical beam passes the reflector strip to reach the next beam expander, while the other optical beam turns the propagation direction going along the optical waveguide of the beam expander. It must be noted that optical sub-beams have different optical paths (see arrows in Fig. 1) and have to interfere (taking into account relevant amplitudes and phases) in order to form the resulting optical beam in the array of the crossing waveguides, or at the output of the Drop beam expander. The result of this interference strongly depends on the position and optical properties of the reflectors, as well as on the optical wavelength. At a particular optical wavelength, all sub-beams constructively interfere, adding up in phase along the axis (*X* in Fig. 1) of the Drop beam expander, and thus providing high intensity Drop signal. At the same optical wavelength, all sub-beams compensate each other in the crossing direction and consequently only a small part of the power comes to the next beam expander (Add). At every other optical wavelength, the condition of constructive interference along the Drop beam expander waveguide is broken and a very small signal comes to the Drop output of the device. Thus, consistently optical sub-beams pass the Drop beam expander, going further with a small energy loss. The typical simulations of MR-ROADM by 2D FDTD are shown in Figs. 11 and 12.

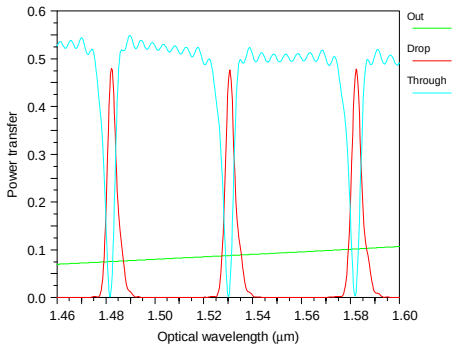

Fig. 11. 2D FDTD simulation of MR-ROADM frequency response with 16 slanted reflectors (φ = 45°) for TM polarization. FWHM = 4.3 nm. FSR = 50 nm. W = 4 μm, n(reflector)= 1.447, d_x = 8 μm, d_z = 16 μm. Variable reflector width from 30 nm to 80 nm.

In order to provide high sidelobe suppression (SLS) and same efficiency for Drop and Through signals, we have monotonically changed the widths of all reflectors, ranging from 30 nm to 80 nm (apodization technique). Figure 11 illustrates the frequency response of multiplexer with rectangular architecture (incident angle φ = 45°), in case of 16 slanted reflectors in every beam expander At particular optical wavelengths, we have a maximum signal at Drop output and high signal rejection at Through one. Figure 2(a) shows that at this wavelength the most of optical signals, coming from the left part of the first (In) waveguide, are added in phase and directed to the Drop output (the second waveguide). At the same time, all the signals compensate each other along the last waveguide (Through) and only a small signal goes to the Through output. For each other wavelength, the constructive interference along the Drop waveguide is broken and all optical signals from the input In goes further to the Through output, as it is shown in Fig. 12(b). These results demonstrate that a device with variable reflector coefficients could well realize the Drop/Through function. Better performance could be provided by a device with larger number of reflectors (> 100), being

#90953 - $15.00 USD Received 17 Dec 2007; revised 25 Jan 2008; accepted 28 Jan 2008; published 21 Feb 2008

their reflection coefficients and positions optimized according with required responses of Drop and Through signals [11]. The requested number of reflectors is typically proportional to the ratio between signal free spectral range (FSR) and full width half maximum (FWHM).

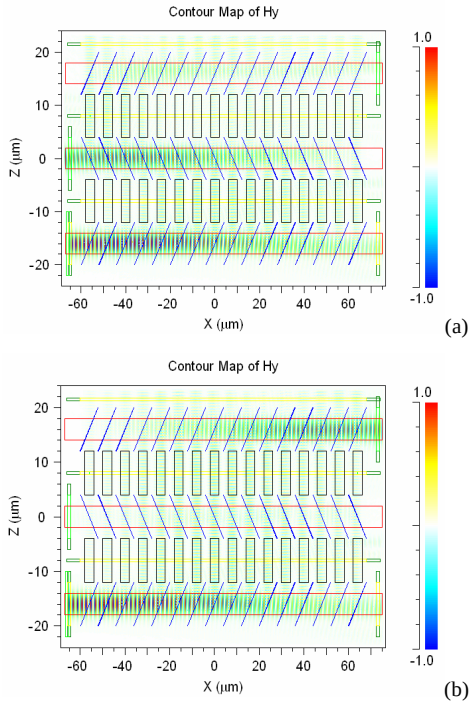

Fig. 12. 2D FDTD simulation of MR-ROADM with 16 slanted reflectors (φ = 45°) for TM polarization. (a) Optical beam propagation at **Drop** wavelength (1.482 μm), (b) Optical beam propagation at **Through** wavelength (1.4925 μm). FWHM = 4.3 nm. FSR = 50 nm. W = 4 μm, n(reflector)= 1.447, d_x = 8 μm, d_z = 16 μm. Variable reflector width from 30 nm to 80 nm.

In general, MR-ROADM needs the implementation of small area bends. Deep grooves in the waveguide with heavy doped sides provide very small optical losses because of the large bend angles obtained by corner reflection, as it can be seen in Fig. 13. Corner reflection produces the additional shift of the middle of reflected beam that can introduce additional losses. To compensate its influence, an additional transverse waveguide shift (*D2*) has been considered in the structure design. Fig. 13 shows that the reflected power is very high for all practically needed incident angles and besides it could be maximized by appropriate waveguide shift. A slanted architecture of MR-ROADM [14], where the beam expanders are tilted of an angle θ $(30< \theta <60)$ relative to X-axis, is also very interesting for practical implementation. It provides a high increase of tuning rate $(\partial\lambda/\partial T)$, that is σ times larger in comparison with any other thermo-optic device on the same material, where $\sigma = 1/(1-\sin(\theta))$ [14].

#90953 - $15.00 USD Received 17 Dec 2007; revised 25 Jan 2008; accepted 28 Jan 2008; published 21 Feb 2008

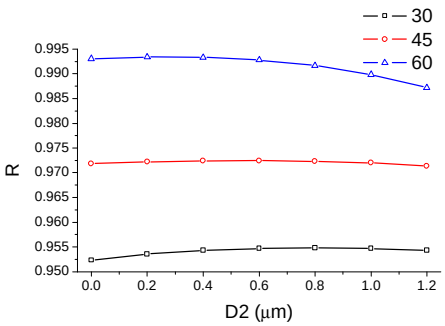

Fig. 13. Dependence of the corner reflection as a function of the waveguide shift (*D2*) at different incident angles (30°, 45°, 60°). 2D FDTD simulation.

All presented results help to develop new MR-ROADM designs of MR-ROADM utilizing 2D-gratings, heavy p^+-doping and nano-scale grooves. The general idea of this design is presented in Fig. 14, which allows the polarization diversity of the device to be achieved. Different polarizations will be coupled by 2D-grating in different directions and filtered by two simultaneously tuned identical ROADMs with hundreds of reflectors. Figure 14 describes a small part of the multiplexer design. We underline that device will have a great number of waveguides and reflectors that are processing the filtering function by multiple interference of sub-beams, each one passing through reflectors and array of heterogeneous waveguides.

Conclusions

This paper presents the first description and simulation of novel nano-photonic SOI waveguide structures providing CMOS compatible manufacturability of multi-reflector reconfigurable optical add/drop multiplexers (ROADMs), based on multi-reflector beam expanders and thermo-optic phase shifters. New structure design includes p^+-doping on both sides of SOI thin ridge waveguide with a 220 nm×16 μm silicon cross section, surrounded by silica cladding. It provides small optical losses for fundamental quasi-TE mode and large losses for higher order modes, due to different free charge absorption depending on the modes field distribution. Nano-grooves etched at Brewster angle with respect to SOI ridge waveguide with p^+-regions provide small reflection coefficients for quasi-TE mode, simplifying the fabrication of multi-reflector ROADMs. Incorporation of these novel structures with 2D nano-grating couplers provides new opportunity for polarization diversity of ROADM. This new SOI structure design could be also interesting for use in other multiple photonic devices.

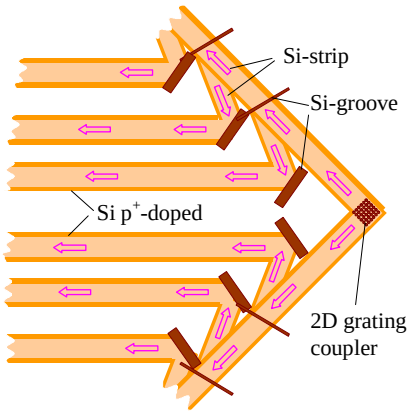

Fig. 14. Part of general design of nano-scale SOI MR-ROADM.

#90953 - $15.00 USD Received 17 Dec 2007; revised 25 Jan 2008; accepted 28 Jan 2008; published 21 Feb 2008

Acknowledgments

The authors thank Company RSoft Design Group, Inc. for providing user license and technical support for Rsoft Photonic CAD Suite ver. 8.0 (including BeamProp 8.0 and FullWave 6.0). This work was partially supported by II Engineering Faculty of Politecnico di Bari with funds by Provincia di Taranto, Italy.

#90953 - $15.00 USD Received 17 Dec 2007; revised 25 Jan 2008; accepted 28 Jan 2008; published 21 Feb 2008